https://dx.doi.org/10.22161/ijaers.76.43 ISSN: 2349-6495(P) | 2456-1908(O)

The use of duplex stainless steel filler metals to avoid hot cracking in GTAW welding of austenitic stainless steel AISI 316L

André de Albuquerque Vicente[1,2], Peter Aloysius D'silva[2], Roberto Luiz de Souza[2], Italo Leonardo dos Santos[2], Renato Rodrigues de Aguiar[2], Amilton Barbosa Botelho Junior[1]

[1]Department of Chemical Engineering, Universidade de São Paulo, Rua do Lago,250, Cidade Universitária, São Paulo, SP, Brazil
[2]ESAB Middle East & Africa, Plot No. S20134, Jebel Ali Free Zone (South), PO Box 8964, Dubai, United Arab Emirates

Abstract *— Sulfur is an element that is intrinsically and sometimes even deliberately present in stainless steel. It is usually bonded in the form of manganese sulfides, which at low levels can have a significant influence on improving machinability. In this work, solidification cracking in austenitic stainless steels welds was investigated. The solidification mode of stainless steels is of fundamental importance and most austenitic stainless steels are designed to solidify to give primary ferrite and secondary austenite to minimize the occurrence of hot cracks. The primary austenitic solidification mode enables cracks to initiate and propagate more easily. This is further enhanced by sulfur segregation. The primary ferritic mode of solidification, however, inhibits crack initiation and propagation and promotes backfilling. The ability to backfill the cracks also affects the extent of cracking observed in welds. Different filler wires were tested to weld, through GTAW welding process, tubes of type 316L UNS S31603 to forged fittings of type ASTM A182 F316 that presented sulfur and phosphorous contents, respectively, 0.03% and 0.045% wt. Duplex stainless steel filler metals ER 2209 and ER 2594, represented a creative solution to avoid hot cracking observed on those samples welded using austenitic stainless steel filler metals ER 316L and ER 309L. Several complementary techniques of microstructural analysis were used, such as optical emission spectrometry, optical microscopy and scanning electron microscopy with coupled EDS*

Keywords *— **Austenitic Stainless Steels; Solidification Mode; Hot Cracking.***

I. INTRODUCTION

The addition of sulfur to ease machinability of stainless steels is largely used by steel shops. Sulfur forms compounds in the stainless steels that will help to break stainless steel chip during machining and form a lubrication layer on the top of the cutting tool, reducing friction and extending tool life. The use of sulfur expanded throughout the stainless industry to give rise to free machining grades such as 303, 416 and 420F.

Certain alloying elements in stainless steels, such as sulfur, selenium, lead, copper, aluminum, calcium, or phosphorus can be added or adjusted during melting to alter the machining characteristics. These alloying elements serve to reduce the friction between the workpiece and the tool thereby minimizing the tendency of the chip to melt and stick to the tool. Also, sulfur forms inclusions that reduce the friction forces and transverse ductility of the chips, causing them to break off more readily. Figure 1 shows the improvement in machinability in the free-machining stainless steels namely types 303, 303 Se, 203, 430F, 416, and 420F. **[1,2]**

https://dx.doi.org/10.22161/ijaers.76.43 *ISSN: 2349-6495(P) | 2456-1908(O)*

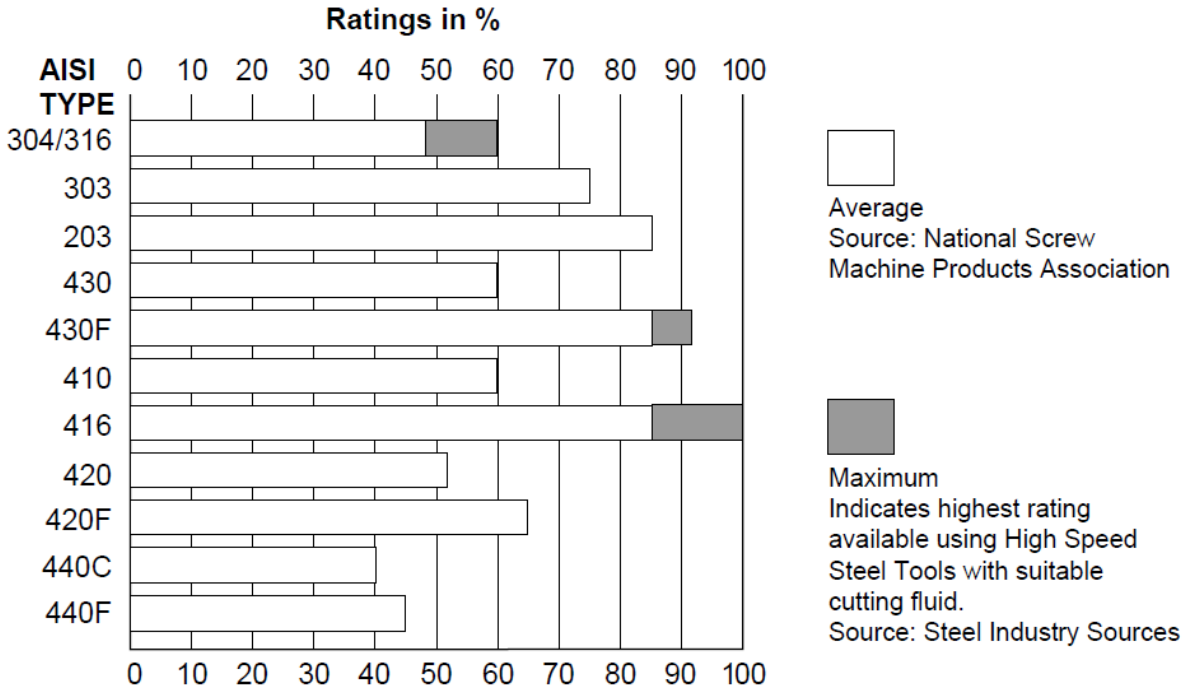

Fig.1: Comparative machinability of frequently used stainless steels and their free-machining counterparts. % based on 100% for AISI type 416 free-machining stainless steel [1]

However, there is a dark side to these high sulfur additions. Sulfur attacks the good attributes of stainless steels. Corrosion is compromised, interferes with welding and can become an initiation site for cracking to occur, especially when any deformation is performed on the part or when there are thin wall sections. The use of sulfur also found its way into other common stainless grades like 410, 304/304L and 316/316L. The adverse effects of sulfur in these grades are not as pronounced on properties as the free machining grades. Welding, corrosion resistance and ductility are generally not an issue. These small sulfur additions do have a substantial effect on the machinability of the stainless steels, as a 0.005% in weight increase can improve machinability by 30% or more. **[1,2]**

The possible solidification modes in the Fe-Cr-Ni system are:

I) ***Austenitic solidification (L → L+γ → γ):***
The only solid phase to form is austenite. In austenitic solidification, called solidification mode I, there is no other phase transformation at high temperature. **[3-5]**

II) **Austenitic-ferritic solidification *(L → L+γ → L+γ+δ → γ+δ):***
Austenite solidifies as a primary phase in a dendritic or cellular way. As the temperature decreases, ferrite δ is formed from the remaining liquid. Solidification occurs through a peritectic reaction (L+δ→γ). This is called solidification mode II. **[3-5]**

III) ***Ferritic-austenitic solidification (L→L+δ→L+δ+γ→δ+γ):***
The duplex stainless steels solidify according to ferritic-austenitic solidification (L→L+δ→L+δ+γ→δ+γ). δ ferrite solidifies as the primary phase in dendritic or cellular fashion. As temperature decreases, austenite is formed by a peritectic (L+δ→γ) or eutectic (L→δ+γ) reaction. In the case of a peritectic reaction, the initially formed austenite completely surrounds the ferrite and subsequently grows into ferrite and liquid. Depending on the rate of diffusion through the austenite, the reaction may or may not be complete, and at the end of the solidification ferrite may be involved in austenite. Between the two reactions - peritectic and eutectic - the transition takes place where, during the initial formation of austenite by peritectic reaction, ferritizing elements secrete to the liquid, provoking their enrichment in these elements and consequently the simultaneous formation of ferrite and austenite by means of a eutectic reaction. This is called solidification mode III. **[3-13]**

IV) ***Ferritic solidification (L→L+δ→δ):***
The only solid phase to form is ferrite. In ferritic solidification, called solidification mode IV, ferrite is

https://dx.doi.org/10.22161/ijaers.76.43 *ISSN: 2349-6495(P) | 2456-1908(O)*

the only phase to form during solidification and, depending on the chemical composition, austenite can precipitate only in the solid state in the ferritic grain boundaries. **[3-5]**

The solidifications of austenitic stainless steels can occur according to the first three solidification modes, being therefore possible to obtain a "completely austenitic" matrix according to the Fe-Cr-Ni equilibrium diagram shown in figure 2.

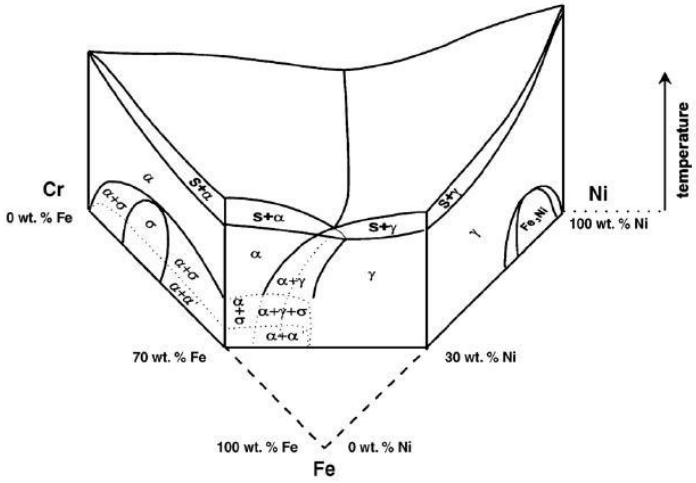

Fig.2: Fe-Cr-Ni ternary phase diagram highlighting the pseudo-binary Cr-Ni diagram for 70% Fe. [6]

Figure 3 presents the Fe-S equilibrium diagram and respective solubility limits of sulfur in the allotropic phases of iron, δ ferrite and γ austenite.

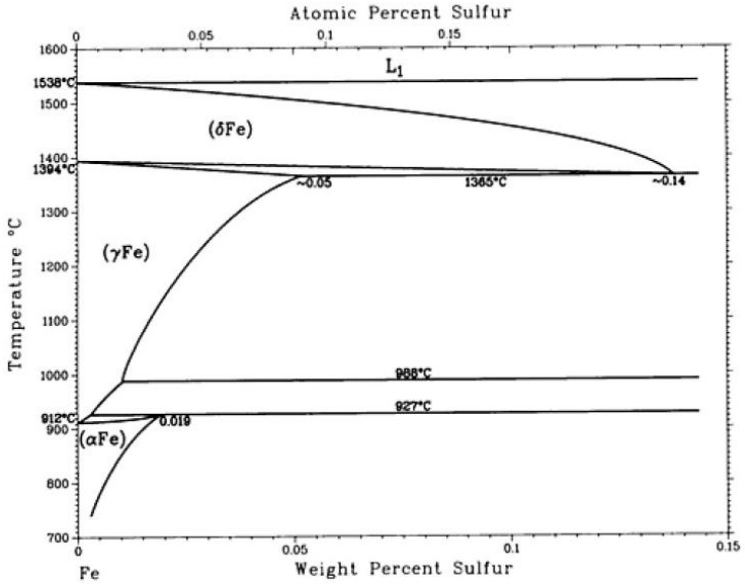

Fe-S crystallographic data

Phase	Composition, wt% S	Pearson symbol	Space group
(δFe)	0 to ~0.14	*cI2*	$Im\bar{3}m$
(γFe)	0 to ~0.05	*cF4*	$Fm\bar{3}m$

Fig.3: Fe-S equilibrium diagram showing solubility limits of sulfur in δ ferrite and γ austenite [14]

It is observed in figure 3 that the solubility limit of sulfur in δ ferrite is 0.14 % in weight and in γ austenite is 0.05 % in weight.

Figure 4 presents the Fe-P equilibrium diagram and respective solubility limits of phosphorus in the allotropic phases of iron, α ferrite and γ austenite.

https://dx.doi.org/10.22161/ijaers.76.43 *ISSN: 2349-6495(P) | 2456-1908(O)*

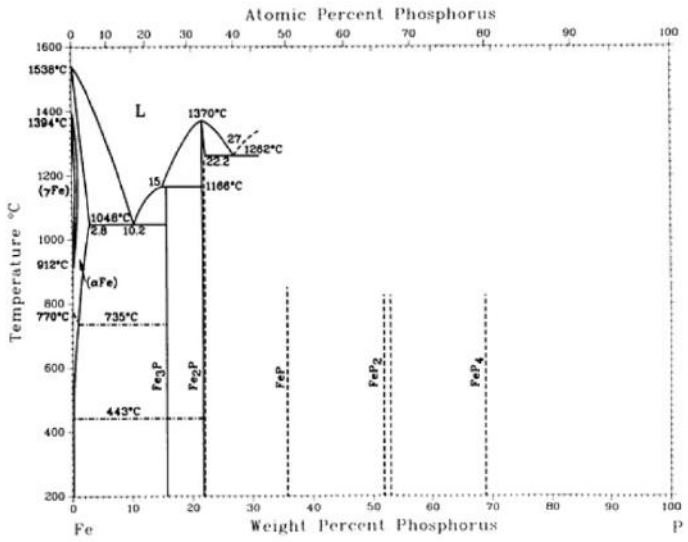

Fe-P crystallographic data

Phase	Composition, wt% P	Pearson symbol	Space group
(γFe)	0 to 0.31	*cF4*	$Fm\overline{3}m$
(αFe)	0 to 2.8	*cI2*	$Im\overline{3}m$

Fig.4: Fe-P equilibrium diagram showing solubility limits of phosphorus in α ferrite and γ austenite [14]

It is observed in figure 4 that the solubility limit of phosphorus in α ferrite is 2.80 % in weight and in γ austenite is 0.31 % in weight.

The information taken from both Figures 3 and 4, helps to understand why solidification cracking is a significant problem during the welding of austenitic stainless steels, particularly in solidification modes I, austenitic solidification, and II, austenitic-ferritic solidification. Hot cracking in stainless steel welds is caused by low-melting eutectics containing impurities such as sulfur and phosphorus, and alloy elements such as titanium and niobium. **[15]**

Sulfur is known to be an undesirable impurity in welding of stainless steels due to the formation of low-melting sulfide films along the interdendritic and grain-boundary regions. Sulfur is strongly rejected into the liquid during solidification of austenite, rapidly lowering the melting point of the interdendritic liquid. Thus, the potential for forming low-melting eutectics remains strong even with very low contents of sulfur in austenite (< 0·005 wt.%). On the other hand, δ-ferrite shows higher solubility for elements like sulfur, phosphorus, silicon and niobium. **[15]**

Manganese additions are well-known to decrease cracking in steels that present high content of sulfur by forming higher-melting MnS-γ eutectic in preference to Fe-FeS. Further, the addition of lanthanum and other rare earth elements has been found highly effective in binding the P and S as stable compounds. **[15]**

Table 1 presents the most important eutectic reactions involving sulfur and phosphorus during the solidification of commercial stainless steels.

Table.1: Partition coefficients of elements promoting hot cracking in austenite and ferrite, constitution and melting points of possible low-melting phases. [15]

Constituent	**Temperature (K)**	**Partition coefficient**		**Low-melting phases**	
		δ	**γ**	**Structure**	**Melting point (K)**
Sulfur	1638	0.091	0.035	**Eutectic Fe–FeS**	1261
				Eutectic Ni–NiS	903
Phosphorus	1523	0.23	0.13	**Eutectic Fe–Fe_3P**	1321
				Eutectic Ni–Ni_3P	1148

Most of the compositions of commercial stainless steels, are in the iron-rich side of the ternary Fe-Cr-Ni equilibrium diagram, between 50 and 70% of iron in weight. The initial solidifying phase is determined by the position of the alloy

https://dx.doi.org/10.22161/ijaers.76.43 *ISSN: 2349-6495(P) | 2456-1908(O)*

with respect to the liquidus surface, which under equilibrium conditions proceeds toward the eutectic/peritectic before solidification is complete. Figure 5 shows the pseudo-binary equilibrium diagram on the vertical section of Fe–Cr–Ni equilibrium diagram at a constant Fe content of 70% in weight. It is commonly used to identify the primary solidifying phases or solidification modes for various compositions of different stainless steels. **[3, 4, 15]**

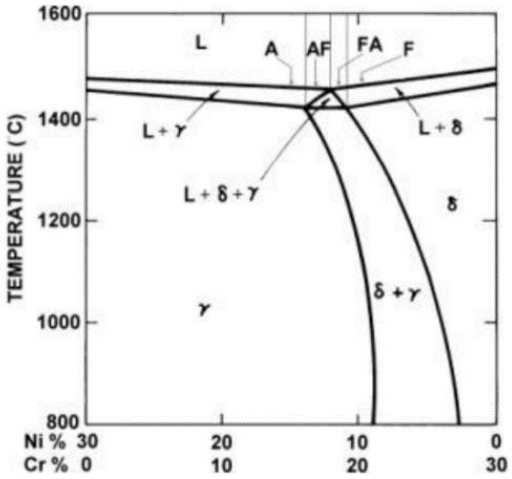

Fig.5: Pseudo-binary section of the Fe–Cr–Ni ternary diagram at 70% Fe, showing solidification modes; A - fully austenitic, AF - austenitic–ferritic, FA - ferritic–austenitic and F - fully ferritic. [15]

When the Cr_{eq}/Ni_{eq} ratio < 1.5, the solidification may be austenitic (mode I) or austenitic-ferritic (mode II). When the ratio 1.5 < Cr_{eq}/Ni_{eq} < 2.0 the solidification will be ferritic-austenitic (mode III). And finally, when Cr_{eq}/Ni_{eq} ratio > 2.0 the solidification will be ferritic (mode IV). **[3]**

Sulfur is known to be an undesirable impurity in welding of stainless steels due to the formation of low-melting sulfide films along the interdendritic and grain-boundary regions. Sulfur is strongly rejected into the liquid during solidification of austenite, rapidly lowering the melting point of the interdendritic liquid. Thus, the potential for forming low-melting eutectics remains strong even with very low contents of sulfur in austenite (< 0·005 wt.%). On the other hand, δ-ferrite shows higher solubility for elements like sulfur, phosphorus, silicon and niobium. **[15]**

Manganese additions are well-known to decrease cracking in high-S steels by forming higher-melting MnS-γ eutectics in preference to FeS. Further, the addition of lanthanum and other rare earths has been found highly effective in binding the P and S as stable compounds. **[15]**

According to studies by Suutala **[16-21]**, the Cr_{eq}/Ni_{eq} ratio is fundamental in determining the solidification mode of austenitic stainless steels.

Figure 6 presents the solidification cracking behavior in austenitic stainless steels welds as a function of Cr_{eq}/Ni_{eq} ratio and P+S levels.

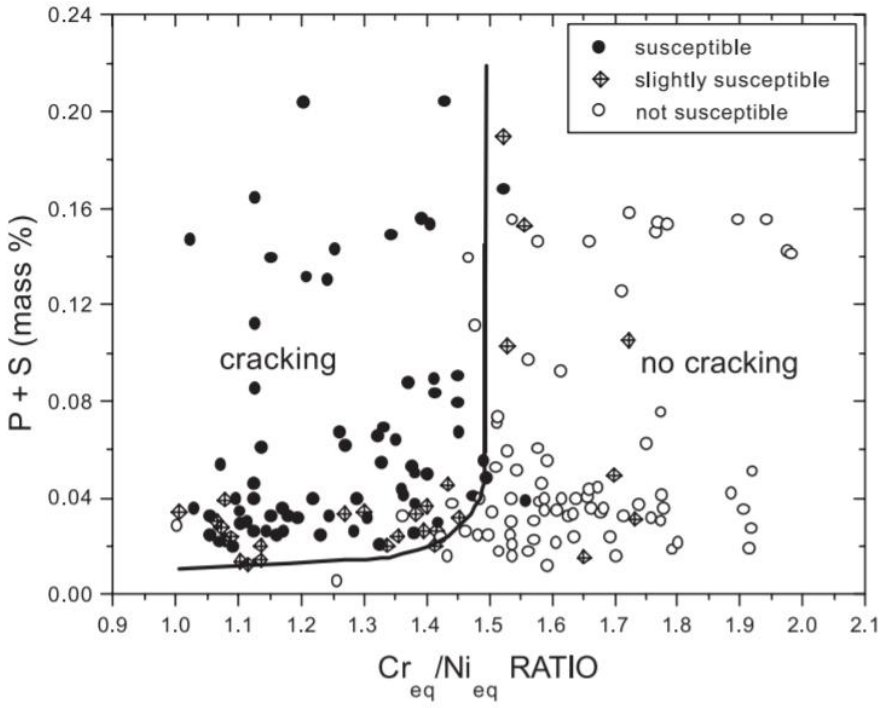

Fig.6: Solidification cracking behavior in austenitic stainless steels welds as a function of Cr_{eq}/Ni_{eq} ratio and P+S levels.[18]

https://dx.doi.org/10.22161/ijaers.76.43 *ISSN: 2349-6495(P) | 2456-1908(O)*

It is observed in figure 6 that austenitic stainless steels that present P+S wt% below 0.01%, are not susceptible to hot cracking. When the Cr_{eq}/Ni_{eq} ratio is below 1.5, if the total P+S wt % is higher than 0.01%, the austenitic stainless steels welds are very susceptible to hot cracking. If $1.5 < Cr_{eq}/Ni_{eq} < 1.75$, the austenitic stainless steels welds are slightly susceptible to hot cracking. Finally, when the Cr_{eq}/Ni_{eq} ratio is higher than 1.75, the austenitic stainless steels welds are not susceptible to hot cracking even for total P+S wt % higher than 0.20.

The Suutala Diagram **[18]**, shown on figure 6, considers the Cr_{eq} and Ni_{eq} are according to the formulas proposed by Hammar and Svensson **[23,24]**:

$$Cr_{eq} = \%Cr+1.37*\%Mo+1,50*\%Si+2,00*\%Nb+3,00*\%Ti$$

(Equation 1) [3]

$$Ni_{eq} = \%Ni+0.31\%Mn+22.00*\%C+14.20*\%N+1.00*\%Cu$$

(Equation 2) [3]

One way of empirically quantifying pitting corrosion resistance is through the PREN (*Pitting Resistance Equivalent Number*), $PREN_N$ (equation 1) and $PREN_W$ (equation 2), when dealing with materials having Tungsten (W) in their composition. **[3]**

$$PREN_N = \%Cr + 3,3\ x(\%Mo) + 16x(\%N)$$

(Equation 3) [3]

$$PREN_W = \%Cr + 3,3\ x(\%Mo + 0,5\ \%W) + 16x(\%N)$$

(Equation 4) [3]

II. EXPERIMENTAL

Four pairs of tubes of type 316L UNS S31603, and forged fittings of type ASTM A182 F316 (weldolets), from the same heats, were welded with different welding wires through GTAW process but keeping the welding parameters as equal as possible.

The tubes are 2 inches diameter and thickness 2,77 mm (SCH 10).

The welding wires used to produce samples 1, 2, 3 and 4 were, respectively, ER 316L, ER 309L, ER 2209 and ER 2594 2.4 mm.

The shielding gases used were 99.99% Ar to samples 1 & 2, 98% Ar+2% N_2 to samples 3 & 4, and the purge gas used was the same 99.99% Ar to all the samples.

The specimens were removed from the base metal and the joints of the tubes using a cut-off.

Chemical analyzes were carried out in all samples by means of an optical emission spectrometer, according to ASTM E 1086-08. **[24]**

Afterwards, the samples were embedded in hot-cure resin (bakelite). The conventional manual polishing was applied using water slicks (100, 240, 320, 400, 600 and 1000 mesh) in order to standardize the surface finish of the samples. Afterwards, a cloth polishing with 9, 3 and 1 μm diamond abrasive paste was carried out in this sequence. The samples were electrolytically attacked in 20% NaOH solution, 6V, for 90 seconds. This allowed the microstructural characterization of the samples through optical microscopy. The quantitative metallographic analyzes for the determination of volumetric fractions of δ ferrite and austenite were performed according to ASTM E 562 ed. 08, **[25]** using a 4 X 5 grid (20 points) with a magnification of 400 X in 30 different regions per test piece.

Finally, tensile tests were performed on welded joints to evaluate their mechanical properties. The preparation of the sub-size specimens to the tensile test was according to ASTM E8/E8M-16ae1 **[26]**.

III. RESULTS AND DISCUSSION

Table 2 presents the welding parameters used to weld the samples. It is important to emphasize that the welding wires used to produce samples 1, 2, 3 and 4 were, respectively, ER 316L, ER 309L, ER 2209 and ER 2594, all 2.4 mm diameter.

Table 2 – Welding parameters used to weld samples 1, 2, 3 and 4 using the filler metals, respectively, ER 316L, ER 309L, ER 2209 and ER 2594, all 2.4 mm diameter.

	Welding Parameters					
	Tension (V)	**Current (A)**	**Travel Speed (mm/s)**	**Thermal Efficiency (%)**	**Heat Input (kJ/mm)**	**Shielding Gas**
Sample 1	11.0	52	0.40	80	1.14	99.99% Ar
Sample 2	10.0	54	0.40	80	1.08	99.99% Ar
Sample 3	10.5	53	0.40	80	1.11	98% Ar+2% N_2
Sample 4	10.0	55	0.40	80	1.10	98% Ar+2% N_2

https://dx.doi.org/10.22161/ijaers.76.43 *ISSN: 2349-6495(P) | 2456-1908(O)*

Table 3 presents the chemical compositions of the tube, fitting, filler metals and all weld metals of the four joints.

According to the chemical compositions obtained from table 3, table 4 presents the calculations of PREN, Cr_{eq}, Ni_{eq}, Cr_{eq}/Ni_{eq} ratio and total P+S wt %.

The calculation of Cr_{eq}, Ni_{eq} and PREN were done using Equations 1, 2 and 3, respectively.

Table 3 - Chemical compositions of the studied stainless steels (% by weight).

		%C	%Si	%Mn	%P	%S	%Cr	%Ni	%Mo	%Cu	%N
Base Metals	**UNS S31603**	0.030	0.45	1.93	0.019	0.003	16.46	11.96	2.07	0.44	0.06
	F316	0.080	0.72	1.93	0.045	0.03	18.66	13.5	2.5	0.10	0.09
Filler Metals	**ER 316L**	0.025	0.63	1.1	0.012	0.008	18.64	12.23	2.53	0.18	0.03
	ER 309L	0.024	0.61	1.72	0.015	0.013	23.57	13.52	0.11	0.16	0.11
	ER 2209	0.022	0.52	1.62	0.01	0.018	23.01	8.89	3.2	0.17	0.15
	ER 2594	0.010	0.48	0.63	0.021	0.015	26.14	9.57	3.92	0.39	0.24
All Weld Metals	**Sample 1**	0.026	0.59	1.27	0.013	0.007	18.2	12.18	2.44	0.23	0.04
	Sample 2	0.035	0.63	1.76	0.021	0.016	22.59	13.52	0.59	0.15	0.11
	Sample 3	0.023	0.54	1.52	0.01	0.016	22.14	9.56	3.07	0.17	0.13
	Sample 4	0.013	0.51	0.85	0.02	0.015	25.63	10.36	3.16	0.34	0.21

Table 4 - PREN, Cr_{eq}, Ni_{eq}, Cr_{eq}/Ni_{eq} ratio and total P+S (weight %).

		PREN	Cr_{eq}	Ni_{eq}	Cr_{eq}/Ni_{eq}	Total S+P (wt %)
Base Metals	**UNS S31603**	24.25	19.97	14.51	1.38	0.022
	F316	28.35	23.17	17.24	1.34	0.075
Filler Metals	**ER 316L**	27.47	23.05	13.73	1.68	0.020
	ER 309L	25.69	24.64	16.3	1.51	0.028
	ER 2209	35.97	28.17	12.18	2.31	0.028
	ER 2594	42.92	32.23	13.78	2.34	0.036
All Weld Metals	**Sample 1**	26.83	22.44	13.88	1.62	0.020
	Sample 2	26.22	24.34	16.49	1.48	0.037
	Sample 3	34.27	27.15	12.49	2.17	0.026
	Sample 4	39.47	30.71	14.29	2.15	0.034

The results shown on tables 3 and 4, confirm that the four filler metals chosen to run the tests, presented PRENs higher than that of the tube UNS S31603. That resulted in chemical compositions of the all weld metals of the samples 1, 2, 3 and 4 that have PRENs above that of the base metal with lower PREN, that in this study is the tube of Type 316L UNS S31603.

The calculation of the Cr_{eq}/Ni_{eq} ratio, and total P+S wt %, showed that both base metals presented Cr_{eq}/Ni_{eq} ratios below 1.5 and the total P+S wt % higher than 0.01%. The same was observed on the all weld metal of sample 2, welded using the filler metal ER 309L. This is an indication that these austenitic stainless steels are very susceptible to hot cracking.

https://dx.doi.org/10.22161/ijaers.76.43 *ISSN: 2349-6495(P) | 2456-1908(O)*

Although the four all weld metals from samples 1, 2, 3 and 4, showed P+S wt % higher than 0.01%, it is interesting to verify that sample 1 presented Cr_{eq}/Ni_{eq} ratio equal to 1.62 indicating that this joint is slightly susceptible to hot cracking. In the case of samples 3 and 4, welding using duplex and super duplex filler metals, respectively, ER 2209 and 2594, the Cr_{eq}/Ni_{eq} ratios are higher than 1.75, resulting that these dissimilar stainless steels welds, solidify in a ferritic-austenitic (mode III) or ferritic (mode IV) fashions. It is expected that these joints are not susceptible to hot cracking even for total P+S wt % higher than 0.20.

Table 5 presents the results of the mechanical properties of the samples 1, 2, 3 and 4.

Table 5 – Mechanical properties and volumetric fractions of δ ferrite.

		Yield Strength (Mpa)	Tensile Strength (Mpa)	Elongation (%)	% δ Ferrite
Base Metals	**UNS S31603**	**225**	**528**	**42**	**4**
	F316	**240**	**560**	**32**	**2**
All Weld Metals	**Sample 1**	**200**	**273**	**10**	**7**
	Sample 2	**160**	**241**	**8**	**2**
	Sample 3	**240**	**575**	**40**	**44**
	Sample 4	**243**	**563**	**33**	**47**

Both samples 3 and 4, welded using duplex and super duplex stainless steels filler metals, respectively, ER 2209 and ER2594, showed higher tensile test results than base metals, being in this way considered approved.

In the other hand, both samples 1 and 2 showed lower tensile test results than base metals. As discussed before, both all weld metals of samples 1 and 2 are prone to solidification cracks.

Figure 7 presents the micrographs of the all weld metals of samples 1 and 2.

a) b)

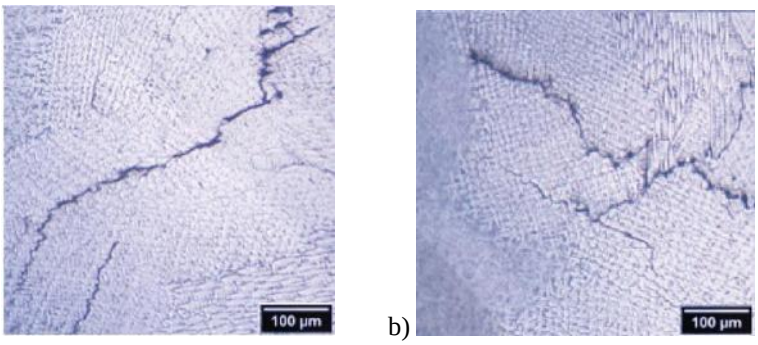

Fig.7 - Micrographs of the all weld metals of a) Sample 1 (ER 316 and b) Sample 2 (ER 309l)

Figures 8 and 9 presents the metallographic analyzes and the respective characterizations of sample 1, as well as the respective semi-quantitative chemical analyzes of regions near and far from the cracks through SEM with coupled EDS.

https://dx.doi.org/10.22161/ijaers.76.43 *ISSN: 2349-6495(P) | 2456-1908(O)*

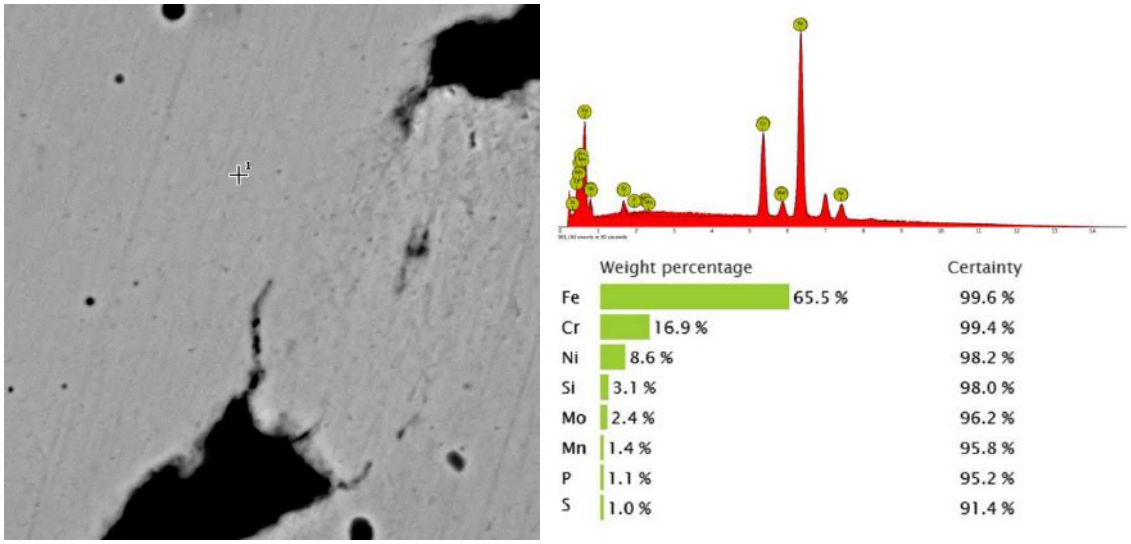

Fig.8 - Metallographic analyzes and respective characterization of Sample1 (All weld metal), as well as, the respective EDS of the region near the cracks.

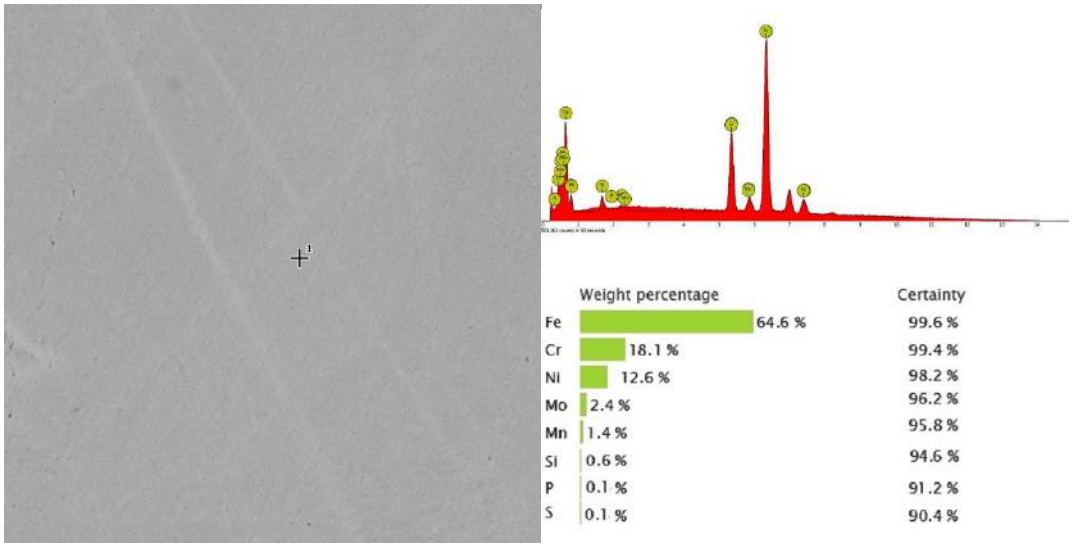

Fig.9 - Metallographic analyzes and respective characterization of Sample1 (All weld metal), as well as, the respective EDS of the region far from the cracks.

The analysis of figures 8 and 9, shows that the regions close to the cracks have higher sulfur and phosphorus contents than the regions away from the cracks.

This fact reinforces the theory that micro segregations of sulfur and phosphorus during the solidification of austenitic stainless steels that present Cr_{eq}/Ni_{eq} ratio below 1.75 can generate solidification cracks.

Austenitic stainless steels are, usually, indicated for high temperature applications **[27]**. However, it is important to emphasize that duplex stainless steels are not recommended for high temperature applications, due to the fact that these stainless steels are prone to the precipitation of deleterious phases, as shown at figure 10.

https://dx.doi.org/10.22161/ijaers.76.43 *ISSN: 2349-6495(P) | 2456-1908(O)*

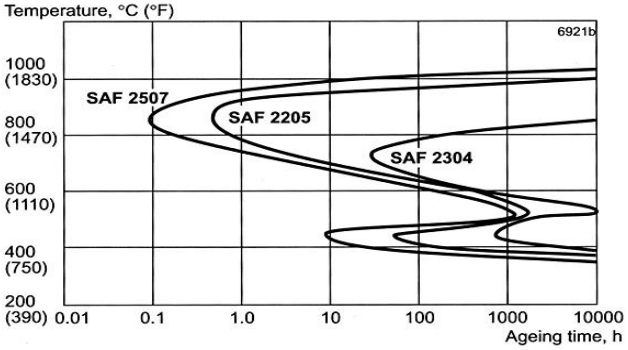

Fig.10 – Time Temperature Transformation (TTT) diagram of duplex stainless steel UNS S32750. [7, 13]

IV. CONCLUSIONS

When the Cr_{eq}/Ni_{eq} ratio is lower than 1.75, the solidification may be austenitic (mode I) or austenitic-ferritic (mode II). If the total content of phosphorous and sulfur is higher than 0.01%, the all weld metal is susceptible to hot cracking.

Sulfur and phosphorous are strongly rejected into the liquid during solidification of austenite, rapidly lowering the melting point of the interdendritic liquid. On the other hand, δ-ferrite shows higher solubility for elements like sulfur, phosphorus, silicon and niobium.

Due to the ferritic-austenitic solidification (mode III), duplex stainless steel filler metals, demonstrate to be efficient in the welding of austenitic stainless steels that present total content of phosphorous and sulfur higher than 0.048%.

REFERENCES

[1] Nickel Development Institute. **Design guidelines for the selection and use of stainless steel, a designer's handbook series, No. 9014.** https://www.nickelinstitute.org/~/Media/Files/TechnicalLiterature/DesignGuidelinesfortheSelectionandUseofStainlessSteels_9014_.pdf

[2] Ahmed, Y. S. **Machinability of Stainless Steels.** Master Thesis. Alexandria University. 2014.

[3] Vicente, A. A.. **Estudo da resistência à oxidação ao ar a altas temperaturas de um aço inoxidável austenítico microligado ao cério soldado pelo processo mig/mag com diferentes gases de proteção.** Tese de Doutorado, Escola Politécnica, Universidade de São Paulo, São Paulo. 2017. https://doi:10.11606/T.3.2017.tde-05092017-103140.

[4] Sindo Kou, **"Welding metallurgy"**, John Wiley & Sons, Inc., 2003, USA. ISBN: 9780471434023.

[5] Vicente, A. A.; Cabral, D. A.; Espinosa, D. C. R.; Tenório, J. A. S.. **Efeito dos gases de proteção na microestrutura e nas cinéticas de oxidação a altas temperaturas ao ar de juntas soldadas de um aço inoxidável austenítico através do processo MIG/MAG**. Tecnol. Metal. Mater. Min., vol.14, n4, p.357-365, 2017. http://dx.doi.org/10.4322/2176-1523.1264.

[6] VICENTE, A. A.; SANTOS, I. L.; JUNIOR, A. B. B.; ESPINOSA, D. C. R.; TENÓRIO, J. A. S.. **Study of the Distribution of Cr, Mo, Ni and N in δ Ferrite and Austenite in Duplex Stainless Steels**. Saudi Journal of Engineering and Technology, 5 (4), 156-162. Scholars Middle East Publishers, Dubai, United Arab Emirates, 2020. https://doi.org/10.36348/sjet.2020.v05i04.005.

[7] VICENTE, A. A.; SOUZA, R. L.; SANTOS, I. L.; AGUIAR, R. R.; PAUL, P.; JUNIOR, A. B. B.. **Effect of relative plate thickness in the heat flow and cooling rate during welding of super duplex stainless steel**. Saudi Journal of Engineering and Technology, 5 (5), 244-150. Scholars Middle East Publishers, Dubai, United Arab Emirates, 2020. https://doi.org/10.36348/sjet.2020.v05i05.005.

[8] Santa-Cruz, L. A., Machado, G., Vicente, A. A. et al. **Effect of high anodic polarization on the passive layer properties of superduplex stainless steel friction stir welds at different chloride electrolyte pH values and temperatures.** Int J Miner Metall Mater 26, 710–721 (2019). https://doi.org/10.1007/s12613-019-1790-0.

[9] Marques, I. J., Vicente, A. D. A., Tenório, J. A. S., & Santos, T. F. D. A. (2017). **Double kinetics of intermetallic phase precipitation in UNS S32205 duplex stainless steels submitted to isothermal heat treatment.** Materials Research, 20, 152-158.

[10] SANTOS, T. F. A.; TORRES, E. A.; LIPPOLD, J.C.; RAMIREZ, A.J. **Detailed microstructural characterization and restoration mechanisms of duplex and superduplex stainless steel friction-stir-welded joints.** J. Mater. Eng. Perform., 25 (2016), 5173-5188. https://doi.org/10.1007/s11665-016-2357-0.

[11] SANTOS, T. F. A.; LÓPEZ, E. A. T.; FONSECA, E. B.; RAMIREZ, A. J.. **Friction stir welding of duplex and superduplex stainless steels and some aspects of microstructural characterization and mechanical performance.** Mater. Res., 19 (2016), pp. 117-131. https://doi.org/10.1590/1980-5373-MR-2015-0319.

[12] Santa Cruz, L. A., Marques, I. J., Urtiga Filho, S .L. et al. **Corrosion Evaluation of Duplex and Superduplex Stainless Steel Friction Stir Welds Using Potentiodynamic Measurements and Immersion Tests in Chloride Environments.** Metallogr. Microstruct. Anal. 8, 32–44 (2019). https://doi.org/10.1007/s13632-018-0506-6.

https://dx.doi.org/10.22161/ijaers.76.43 *ISSN: 2349-6495(P) | 2456-1908(O)*

[13] VICENTE, A. A.. (2011). **Welding Practice for the Sandvik Duplex Stainless Steels for the Sandvik Duplex Stainless Steels SAF 2304, SAF 2205 and SAF 2507.** https://doi.org/10.13140/RG.2.2.19576.39682

[14] ASM Handbook. (1992). Volume 3. Alloy phase diagrams. ASM International. Handbook Committee. Materials Park. Ohio: ASM International.

[15] Shankar, V.; Gill, T.P.S.; Mannan, S.L. et al. **Solidification cracking in austenitic stainless steel welds.** Sadhana 28, 359–382 (2003). https://doi.org/10.1007/BF02706438

[16] SUUTALA, N.; TAKALO, T.; MOISIO, T.. **Ferritic-Austenitic Solidification mode in Austenitic Stainless Welds**. Metalurgical Transactions A, vol 11A, p. 717-725, 1980.

[17] SUUTALA, N.; MOISIO, T.. **Use of chromium and nickel equivalents in considering solidification mode in austenitic stainless steel welds.** Solidification and Casting Metals, London, The Metals Society, p. 310- 314, 1979.

[18] SUUTALA, N.; TAKALO, T.; MOISIO, T.. **The relationship between solidification and microstructure in austenitic-ferritic stainless steel welds.** Metallurgical Transactions A, vol. 10A, p.512-514, 1979.

[19] TAKALO, T.; SUUTALA, N.; et al.. **Austenitic solidification mode in austenitic stainless steel welds.** Metallurgical Transactions A, vol. 10A, p. 1173-1181, 1979.

[20] SUUTALA, N.; TAKALO, T.; et al.. **Single-phase ferritic solidification mode in austenitic-ferritic stainless steel welds.** Metallurgical Transactions A, vol. 10A, p. 1183-1190, 1979.

[21] SUUTALA, N.. **Effect of solidification conditions on the solidification mode in austenitic stainless steels.** Metallurgical Transactions A, vol. 14, p. 191-195, 1983.

[22] HAMMAR, O.; SVENSSON, U.. **Influence of Steel Composition on Segregation and Microstructure During Solidification of Austenitic Stainless Steels.** Solidification and Casting Metals, London, Metals Society, p. 401- 410, 1979.

[23] HAMMAR, O. ; SVENSSON, U.. **A Guide of solidification**. Jernkontoret, Stockholm, p. 269, 1977.

[24] ASTM E1086-08: Standard Test Method for Optical Emission Vacuum Spectrometric Analysis of Stainless Steel by the Point-to-Plane Excitation Technique. ASTM International. West Conshohocken. PA. EUA. 2008.

[25] ASTM E562-08: Standard Test Method for Determining Volume Fraction by Systematic Manual Point Count. ASTM International. West Conshohocken. PA. EUA. 2008.

[26] ASTM E8/E8M-16ae1: Standard Test Methods for Tension Testing of Metallic Materials. ASTM International. West Conshohocken. PA. EUA. 2016.

[27] A. de Albuquerque Vicente, J.R.S. Moreno, D.C.R. Espinosa, T.F. de Abreu Santos, J.A.S. Tenório. **Study of the high temperature oxidation and Kirkendall porosity in dissimilar welding joints between FE-CR-AL alloy and stainless steel AISI 310 after isothermal heat treatment at 1150 °C in air.** J. Mater. Res. Technol. 8(2), 1636 (2019).